Fermi Surface of Three-Dimensional $La_{1-x}Sr_xMnO_3$ Explored by Soft-X-Ray ARPES: Rhombohedral Lattice Distortion and its Effect on Magnetoresistance

L. L. Lev,[1,2,*] J. Krempaský,[1] U. Staub,[1] V. A. Rogalev,[1] T. Schmitt,[1] M. Shi,[1] P. Blaha,[3] A. S. Mishchenko,[4,2] A. A. Veligzhanin,[2] Y. V. Zubavichus,[2] M. B. Tsetlin,[2] H. Volfová,[5] J. Braun,[5] J. Minár,[5,6] and V. N. Strocov[1,†]

[1]*Swiss Light Source, Paul Scherrer Institute, 5232 Villigen, Switzerland*
[2]*National Research Centre "Kurchatov Institute", 123182 Moscow, Russia*
[3]*Institut für Materialchemie, Technische Universität Wien, A-1060 Wien, Austria*
[4]*RIKEN Center for Emergent Matter Science, 2-1 Hirosawa, Wako, Saitama 351-0198, Japan*
[5]*Department Chemie, Ludwig-Maximilians-Universität München, 81377 Munich, Germany*
[6]*New Technologies-Research Center, University of West Bohemia, 306 14 Plzen, Czech Republic*

(Received 11 November 2014; published 9 June 2015)

Electronic structure of the three-dimensional colossal magnetoresistive perovskite $La_{1-x}Sr_xMnO_3$ has been established using soft-x-ray angle-resolved photoemission spectroscopy with its intrinsically sharp definition of three-dimensional electron momentum. The experimental results show much weaker polaronic coupling compared to the bilayer manganites and are consistent with the theoretical band structure including the empirical Hubbard parameter U. The experimental Fermi surface unveils the canonical topology of alternating three-dimensional electron spheres and hole cubes, with their shadow contours manifesting the rhombohedral lattice distortion. This picture has been confirmed by one-step photoemission calculations including displacement of the apical oxygen atoms. The rhombohedral distortion is neutral to the Jahn-Teller effect and thus polaronic coupling, but affects the double-exchange electron hopping and thus the colossal magnetoresistance effect.

DOI: 10.1103/PhysRevLett.114.237601 PACS numbers: 79.60.-i, 71.18.+y, 75.47.Gk, 75.47.Lx

Hole-doped manganites with the general chemical formula $(La, Sr)_xMnO_y$ (LSMO) are typical transition metal oxides (TMOs) with perovskite structure, which have attracted tremendous interest due to the discovery of their colossal magnetoresistance (CMR). Coupling of charge, orbital, spin, and lattice degrees of freedoms results in a rich phase diagram of these materials, extending over antiferromagnetic, ferromagnetic (FM), and paramagnetic (PM) insulating and metallic states. The electron transport in manganites is coupled to their ferromagnetism and is generally described in the framework of the double-exchange (DE) mechanism. However, an important role in physics of these materials can be played by polaronic effects coupling of the electron and lattice degrees of freedom whose driving force is the Jahn-Teller (JT) distortion. According to the theory of Millis *et al.* [1,2], supported by experiments on the bilayer $La_{2-2x}Sr_{1+2x}MnO_7$ manganites [3,4], the competition between the DE related electron itineracy and polaronic self-trapping leads to a crossover from the Fermi liquid regime in the FM metal to the polaronic regime in the poorly conducting PM state at the critical temperature T_c. The CMR occurs then due to the magnetic field shifting the balance of these two effects near the crossover point.

The present study focuses on the LSMO compounds with the composition $La_{1-x}Sr_xMnO_3$ which crystallize in three-dimensional (3D) cubiclike perovskite structures (3D-LSMO) with various lattice distortions including orthorhombic and rhombohedral (RH). The structural difference compared to the layered LSMO compounds immediately affects the polaronic effects. Indeed, the strength of these effects is determined by the electron-phonon interaction characterized by the dimensionless coupling parameter $\lambda_{e\text{-ph}}$ depending on the number of the nearest Mn neighbors z. Namely, $\lambda_{e\text{-ph}} = \sum_m f_m^2(0)/(2zMt\omega^2)$, where f_m are the force functions depending on the chemical bonds of ions, ω is the phonon frequency, and M the oscillator mass [5]. Hence, the 3D-LSMO compounds with their more delocalized electron system compared to the layered LSMO [3] should show significantly smaller polaronic effects because each Mn atom in a 3D compound is coupled by the DE to six Mn neighbors against four in the single-layer $La_{2-x}Sr_xMnO_4$ and five in the bilayer $La_{2-2x}Sr_{1+2x}MnO_7$.

Angle-resolved photoelectron spectroscopy (ARPES) is the most direct method to explore the electronic structure resolved in electron momentum $\mathbf{k}$. The intrinsically 3D nature of the 3D-LSMO compounds is a complication compared to two-dimensional materials such as cuprates or the layered LSMO [3] because the conventional ARPES employing vacuum ultraviolet (VUV) photon energies $h\nu$ below 100 eV suffers from ill definition of surface-perpendicular momentum $k_\perp$ [6] intrinsically limited by non-free-electron final-state dispersions and large final-state broadening $\Delta k_\perp \sim \lambda^{-1}$ connected with small photoelectron escape depth λ of a few Å. Although the previous VUV-ARPES studies [7–12] have established a general picture of the 3D-LSMO electronic structure, this limitation [7,8] as well as the use of thin film samples with their potential

electronic structure distortion near the surface [13] have restricted relevance of the experimental results. Furthermore, the absence of any complete determination of the FS topology left doubts on whether the polaronic (bosonic) coupling could not disintegrate the FS in certain $\mathbf{k}$-space regions, which is one of the scenarios to explain the FS arcs in cuprates [14].

In this Letter, we explore the electronic structure of single-crystal 3D-LSMO with the optimal Sr doping $x = 0.33$ using soft-x-ray ARPES (SX-ARPES) with $h\nu$ up to 1 keV, where the increase of λ towards ~15 Å results in sharp definition of $k_\perp$ and thus 3D momentum [15]. We achieve the most fundamental electronic structure information about 3D-LSMO, including the 3D topology of its FS and strength of electron-polaron coupling, and consolidate these findings with theoretical models. Furthermore, we identify spectroscopic signatures of the RH lattice distortion and analyze its effect on the Jahn-Teller (JT) distortion and CMR effect.

Experiment.—The experiments were performed at the ADRESS beamline of the Swiss Light Source. High photon flux above 10^{13} photon/sec/0.01% combined with the optimized geometry of the SX-ARPES endstation [16] overpowered the dramatic loss of photoexcitation cross-section at soft-x-ray energies (a factor of ~200 for the valence Mn $3d$ states compared to VUV-ARPES) [15]. The combined energy resolution was ~120 meV. The sample was kept at 11 K to avoid the destructive effects of electron-phonon scattering on the coherent ARPES signal [17]. Variations of the emission angle ϑ and $h\nu$ were rendered into $\mathbf{k}$ space with correction for the photon momentum $p^{\mathrm{ph}} = h\nu/c$ [16] and using an empirical inner potential V_0 of 7 eV. The present experimental data were collected with circular x-ray polarization.

Single crystals of $La_{1-x}Sr_xMnO_3$ with the optimal Sr doping $x = 0.33$ were grown by the floating zone method at the Moscow Power Institute. Their electric resistivity and magnetic susceptibility characterization was in agreement with the published data [18]. The crystals were FM metals below $T_C = 360$ K and poorly conducting PM metals above. Structural characterization with x-ray diffraction, see the Supplemental Material [19], has identified their RH-distorted cubic structure. The cubic-lattice equivalent lattice constant is $a = 3.89$ Å, almost independent of temperature. The samples were cleaved *in situ* by an anvil-knife setup. The resulting (001) surfaces were optically rough but well defined electronically as evidenced by clear LEED images without any signs of surface reconstructions.

Theoretical electronic structure.—We used the standard DFT framework with the exchange–correlation functional treated within the generalized gradient approximation (GGA). The local correlation effects necessary to describe the half-metallic nature of 3D-LSMO were introduced via the empirical Hubbard parameter $U = 2$ eV applied to the Mn $3d$ states [8]. The band calculations used the full-potential APW method implemented in the WIEN2K package. The Sr doping randomly replacing La atoms was introduced with the virtual crystal approximation (VCA);

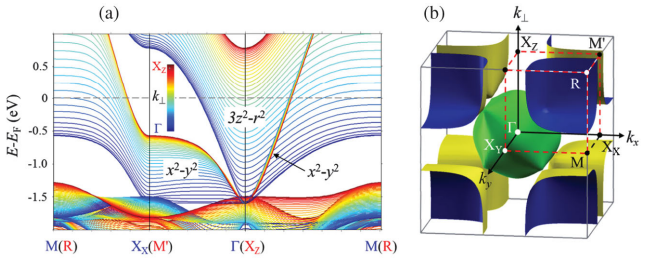

FIG. 1 (color). GGA + U calculations for the ideal cubic structure of 3D-LSMO [7,8]: (a) (Spin-up) band structure, with the color scale indicating $k_\perp$ of the bands; (b) Fermi surface.

for details see Ref. [8]. Figure 1 shows the theoretical band structure $E(\mathbf{k})$ and FS calculated for the ideal cubic structure with $a = 3.89$ Å. As the RH-distortion is relatively weak, these calculations will serve as a road map for our further analysis. The (spin-up) valence bands near the Fermi level E_F are defined essentially by the Mn $3d$ states of the e_g type (almost insensitive to the variations of U) which split into the $3z^2 - r^2$ and $x^2 - y^2$ states and hybridize with primarily the O $2p$ states [20]. The theoretical FS consists of the sphere-like electron pocket (e spheroid) around the Γ point and cubelike hole pockets (h cuboids) centered around the Brillouin zone (BZ) corners. In a perspective of our photoemission analysis, we have also performed the GGA + U calculations using the fully relativistic Korringa–Kohn–Rostoker (KKR) method as implemented in the Munich SPR-KKR code [21] with the Sr doping introduced within the coherent potential approximation (CPA) that correctly reproduces the $E(\mathbf{k})$ smearing due to the disordered nature of 3D-LSMO. The APW + VCA and KKR + CPA calculations yielded indistinguishable band structures.

Experimental band dispersions and polaronic coupling.—The experimental results representing the valence band spectral function $A(\omega, \mathbf{k})$ along two directions in the BZ are shown in Fig. 2 as images of the ARPES intensity depending on binding energy E_B and surface-parallel momentum k_x (along the analyzer slit). To emphasize the dispersive spectral structures, we have subtracted from the raw ARPES intensity its nondispersive component obtained by angle integration, for the raw data see Ref. [19]. The data along the ΓX_X and ΓM lines were measured with $h\nu =$ 643 eV chosen at the main Mn $2p$ absorption peak to resonantly enhance photoemission intensity from the Mn $3d$ valence states. Incidentally, the corresponding $k_\perp$ values (indicated on top of the images) slightly varying with k_x, appear close to $8(2\pi/a)$ at the ΓX_X and ΓM lines. Comparison of the experimental data with the theoretical $E(\mathbf{k})$ in Fig. 1 immediately identifies the e_g bands derived from the $3z^2 - r^2$ orbitals (forming the e spheroid of the FS) and the $x^2 - y^2$ orbitals. In the ΓX_X data, we note that $k_\perp$ comes closest to the exact ΓX_X line in the second surface BZ (marked Γ_1), which results in a visually deeper $3z^2 - r^2$ band compared to the first BZ (Γ_0). In contrast to the previous VUV–ARPES data [7–11] (for a detailed analysis of the differences see Ref. [19]) our experiment shows remarkable

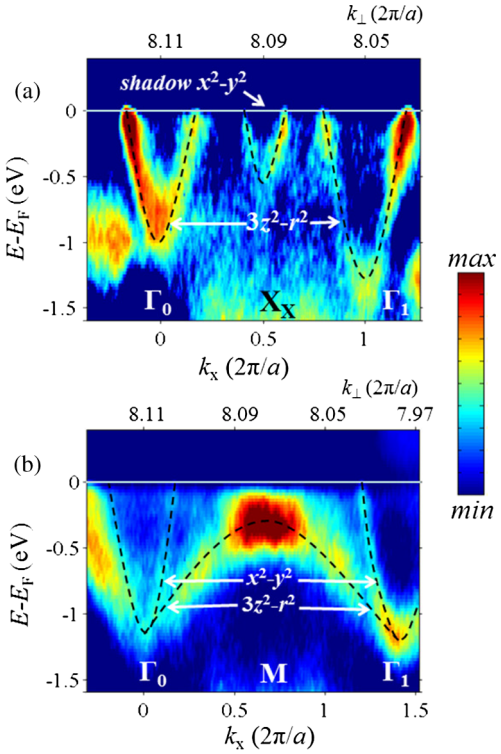

FIG. 2 (color online). Experimental ARPES images representing the ΓX_X (a) and ΓM (b) lines of the BZ measured with $h\nu = 643$ eV (Mn $2p$ resonance). The $k_\perp$ variations are shown on top of the images. The dashed lines are visual guides for the experimental dispersions. The orbital character of the bands is indicated, and the shadow $x^2 - y^2$ band is marked. The experimental bands do not show any significant renormalization compared to the GGA + U bands in Fig. 1(a).

agreement with the GGA + U calculations, Fig. 1(a), with only a slight e_g bandwidth renormalization of around 20%.

ARPES studies of the bilayer compounds $La_{2-2x}Sr_{1+2x}MnO_7$ have found $A(\omega, \mathbf{k})$ having a pronounced peak-dip-hump structure [3] composed of the quasiparticle (QP) peak and polaronic hump. In contrast, our data in Fig. 2—also see the energy distribution curves (EDCs) in Ref. [19]—demonstrate single peaks (albeit broadened beyond the lifetime due to the remnant $\Delta k_\perp$ effects [7,8] and intrinsic disorder of the intermixed La and Sr ions in 3D-LSMO). The peaks disperse up to E_F without any loss of the spectral weight. This identifies them as the QP peaks of $A(\omega, \mathbf{k})$ because the humps, for all known polaronic systems, may disperse but always stay below E_F [3]. This conclusion is confirmed by the ARPES temperature dependence [19]. The hump can only be suspected in slight asymmetry of the spectral peaks, with its vanishing weight being consistent with the insignificant band renormalization. The weak polaronic coupling in 3D-LSMO reflects its 3D nature where electron hopping to a larger number of the nearest Mn neighbors compared to the layered LSMO impedes stabilization of the polarons.

Experimental FS.—Figures 3(a) and 3(b) show the experimental FS maps representing the $\Gamma X_X M$ and $X_Z M' R$ horizontal planes of the BZ. The maps were measured as the ARPES intensity at E_F as a function of the surface-parallel momenta k_x and k_y (the latter varied through the sample rotation). The $\Gamma X_X M$ map was measured again at the Mn $2p$ resonance. We immediately recognize the characteristic circular cuts of the e spheroids around the Γ points expected from the theoretical FS in Fig. 1(b). The $X_Z M' R$ map measured with $h\nu$ varying around 708 eV immediately shows the characteristic cubic cuts of the h cuboids around the R points in Fig. 1(b). We note that the remnant final-state $\Delta k_\perp$ broadening builds up, in the $\Gamma X_X M$ map, the checkerboard intensity enhancements over the M points projected from the h cuboids and, in the $X_Z M' R$ map, the enhancements over the Γ points projected from the e spheroids.

Figures 3(c) and 3(d) show the experimental FS maps measured in the vertical $\Gamma X_X M'$ and $X_Y MR$ planes under variation of $k_\perp$ through $h\nu$. These $k_\perp$ maps show the same characteristic pattern of the spheres and cubes as the above $\mathbf{k}_{//}$ cuts, as expected because of the essentially cubic structure of 3D-LSMO. We only note somewhat larger broadening of the horizontal FS fragments compared to the vertical ones which again manifests the $\Delta k_\perp$ effects. Therefore, the whole body of our results fully confirms the canonical FS topology in Fig. 1(b). To the best of our knowledge, our experiment is the first complete resolution of this most fundamental property of the electronic structure of 3D-LSMO. The FS does not show any evident regions of suppressed intensity, which might otherwise have suggested destructive enhancements of $\mathbf{k}$-dependent polaronic (bosonic) coupling.

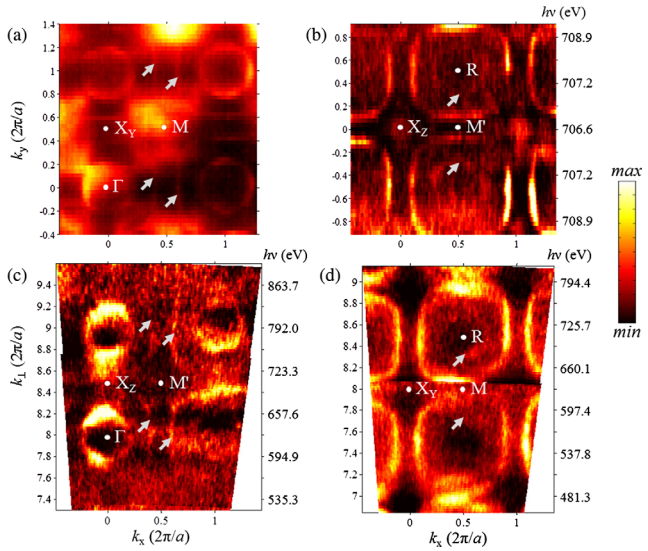

FIG. 3 (color online). Experimental $\mathbf{k}_{//}$ cuts of the FS measured as a function of θ, representing the $\Gamma X_X M$ plane [(a), measured at $h\nu = 643$ eV] and $X_Z M' R$ plane [(b), with $h\nu$ marked on the right varying around 708 eV as a function of k_y to keep constant $k_\perp$]; experimental $k_\perp$ cuts measured under $h\nu$ variations (marked on the right for $k_x = 0$) representing the $\Gamma X_X M'$ (c) and $X_Y MR$ (d) planes. For the latter, $h\nu$ tracked the sample rotation to keep constant $k_y = \pi/a$. The experiment fully confirms the 3D topology of the FS in Fig. 1(b). The shadow FS contours are marked by arrows.

Shadow FS and its origin.—The most intriguing discovery in the experimental FS maps in Fig. 3 are distinct replicas of the h cuboids seen around the e spheroids (most pronounced in the $\Gamma X_X M$ map) and, vice versa, those of the e spheroids inside the h cuboids. They can be represented as a translation of the fundamental FS in Fig. 1(b) with an umklapp vector $(\pi/a, \pi/a, \pi/a)$ along the space diagonal $R\Gamma R$ of the BZ to halve its size. As these replicas can be viewed as a 3D analogue of the similar effect in cuprates [22,23] we will call them also "shadow" FS (SFS). In particular, the umklapp translates the $RM'R$ direction onto the horizontal $\Gamma X_Y \Gamma$ one. Correspondingly, the $x^2 - y^2$ band around the M' point, see Fig. 1(a), produces the shadow band around the X point, Fig. 2(a), to form the SFS h cuboids.

No surface reconstruction could induce this effect, because in that case the corresponding umklapp vector would have been parallel to surface, plus our samples showed no surface reconstructions. An appealing explanation of the SFS would be some hidden magnetic order potentially related to the CMR of 3D-LSMO. Such a possibility has been long debated in connection with the SFS in cuprates [22]. Another possibility would be an orbital and/or charge order [24]. However, the spectroscopic signatures of these two order parameters are normally extremely weak. The most plausible explanation is then some structural effect. We note that the long debated SFS in cuprates has finally proved to have the same origin [23]. Indeed, the structural distortion modes involving tilting of the atomic arrangement in the unit cell of the 3D-LSMO with $x = 0.33$ transform the cubic to RH-distorted lattice structure [25]. The resulting unit cell in Fig. 4(a) doubles the cubic unit cell along the space diagonal, or halves the cubic BZ in the $R\Gamma R$ direction as observed in our experiment. This mechanism is further corroborated by relaxation of the ARPES linear dichroism, which reflects collapsing symmetries of the valence states [19].

This interpretation is confirmed by results of our relativistic one-step photoemission calculations extended to the alloy systems which included the KKR + CPA initial states, photoemission matrix elements and final states effects [26,27]. The embedded RH-distortion model included displacement of the apical oxygen atoms below and above the (001) oriented Mn-O planes (see the structural parameters in Ref. [19]). The ARPES intensity was calculated as $I_{\mathrm{ARPES}} \propto \langle \phi^f_{\mathbf{K}} | \Delta^* \mathrm{Im}\mathbf{G}_i \Delta | \phi^f_{\mathbf{K}} \rangle$, where $\phi^f_{\mathbf{K}}$ represents the final state as the time reversal LEED state, $\Delta = A_0\mathbf{p}$ is the dipole operator where A_0 denotes constant amplitude of the electromagnetic field vector potential and $\mathbf{p}$ is the momentum operator, and the Green's function $\mathbf{G}_i$ represents the initial valence states $\phi^i_{\mathbf{k}}$ [26]. In the simplest approximation this expression represents basically the matrix element weighted projection of $\phi^i_{\mathbf{k}}$ onto the final state represented by the plane wave $\phi^f_{\mathbf{K}} = e^{i\mathbf{Kr}}$ as $I_{\mathrm{ARPES}} \propto \langle e^{i\mathbf{Kr}} | \phi^i_{\mathbf{k}} \rangle$. Therefore, our photoemission analysis is essentially the direct plane-wave projection [28] of the rhombohedral lattice wave functions to yield the valence band $A(\omega, \mathbf{k})$.

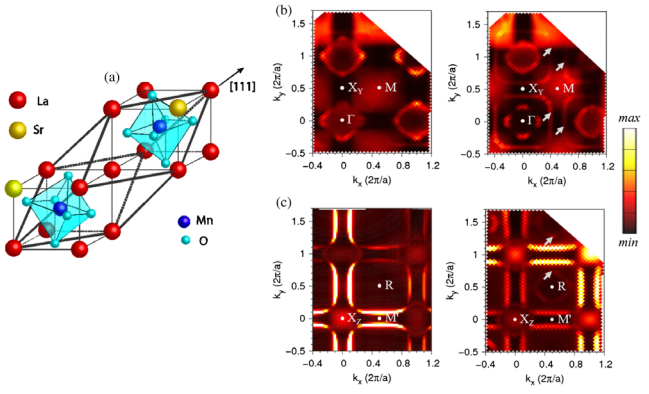

FIG. 4 (color online). (a) RH-distortion of the 3D-LSMO unit cell with Sr randomly substituting La ions; (b),(c) ARPES calculations of the $\mathbf{k}_{//}$ cuts representing the FS in the $\Gamma X_X M$ (b) and $X_Z M'R$ (c) planes for the ideal cubic (left) and RH distorted crystal lattice (right). The calculations confirm the structural origin of the SFS marked by arrows.

Figures 4(b) and 4(c) show our ARPES calculations of the FS maps in the $\Gamma X_X M$ and $X_Z M'R$ planes for the ideal cubic and RH-distorted lattice. As expected, for the cubic case these maps show the canonic FS contours identical to the GGA + U calculations in Fig. 1(b). Notably, perfectly reproduced are the $\Delta k_\perp$ effects, the projections of the h cuboids in the $\Gamma X_X M$ plane and those of the e spheroids in the $X_Z M'R$ plane. When we turn on the RH-distortion, we immediately see the contours of the SFS h cuboids and e spheroids in complete agreement with the experiment in Figs. 3(a) and 3(b), not only on their position but also relative intensities. Our calculations therefore confirm the RH lattice distortion as the origin of the SFS.

Connection of the RH-structural distortion with the JT distortion.—On first glance, the atomic displacements caused by the RH-distortion should change the atomic force constants and therefore the strength of the polaronic coupling. However, this distortion leads the manganese ion to a local symmetry of $\bar{3}$ which splits the t_{2g} levels but does not remove the degeneracy of the $3z^2 - r^2$ and $x^2 - y^2$ states forming the FS. The RH-distortion does not therefore affect the JT activity and polaronic coupling in the first order, with the higher-order corrections being less important. On the other hand, although the RH-distortion hardly changes the length of each Mn-O bond, it reduces the Mn-O-Mn angle from an ideal 180° to a significantly smaller value of 166.46°, which weakens the DE interaction between the two Mn atoms (expressed by the effective electron hopping t_{eff}) and thus reduces the electron itineracy. According to the theory of Millis *et al.* [1,2], the crossover from the FM metal to the poorly conducting PM metal occurs when electron itineracy is prevailed by the polaronic self-trapping. The RH-distortion has therefore an effect to shift the CMR to lower T_c. In this respect, the RH-distortion acts opposite to the trend when going from the layered LSMO compounds to the 3D ones where the increase of dimensionality and coordination number of the Mn-O-Mn bonds facilitates the electron hopping and thus suppresses the polaronic self-trapping.

Conclusion.—We have explored the electronic structure of 3D-LSMO using SX ARPES with its intrinsically sharp definition of 3D electron momentum and single-crystal samples free of the surface reconstructions. The experimental valence band $A(\omega, \mathbf{k})$ demonstrates considerably weaker electron-polaron coupling compared to the bilayer LSMO compounds. Obscured in the previous VUV-ARPES studies, the experimental FS appears as the canonic 3D manifold of electron e spheroids and h cuboids predicted by GGA + U band calculations. Apparent shadow FS structures, analyzed with one-step photoemission calculations, prove to manifest the RH lattice distortions rather than any magnetic or orbital order. The RH-distortion is neutral to the JT effect and thus polaronic coupling, but reduces the electron itineracy and therefore acts to shift the CMR to smaller T_C.

We thank V. A. Gavrichkov for promoting discussions, A. M. Balbashev for giving us access to single crystals, and S. S. Johnston for expert advice on polaronic physics. J. M. was supported by the Deutsche Forschungsgemeinschaft through Grant FOR 1346, the BMBF (Project 05K13WMA), and CENTEM (CZ.1.05/2.1.00/03.0088). J. M. and P. B. thank European COST network Euspec (MP1306) for support. A. S. M. acknowledges the support of ImPACT Program of Council for Science, Technology and Innovation (Cabinet Office, Government of Japan).

*lll_ru@mail.ru
†vladimir.strocov@psi.ch

[1] A. J. Millis, B. I. Shraiman, and R. Mueller, Phys. Rev. Lett. **77**, 175 (1996); A. J. Millis, Nature (London) **392**, 147 (1998).
[2] C. Hartinger, F. Mayr, A. Loidl, and T. Kopp, Phys. Rev. B **73**, 024408 (2006).
[3] Y. Moritomo, A. Asamitsu, H. Kuwahara, and Y. Tokura, Nature (London) **380**, 141 (1996); N. Mannella, W. L. Yang, X. J. Zhou, H. Zheng, J. F. Mitchell, J. Zaanen, T. P. Devereaux, N. Nagaosa, Z. Hussain, and Z.-X. Shen, Nature (London) **438**, 474 (2005); F. Massee, S. de Jong, Y. Huang, W. K. Siu, I. Santoso, A. Mans, A. T. Boothroyd, D. Prabhakaran, R. Follath, A. Varykhalov, L. Patthey, M. Shi, J. B. Goedkoop, and M. S. Golden, Nat. Phys. **7**, 978 (2011).
[4] N. Mannella, A. Rosenhahn, C. H. Booth, S. Marchesini, B. S. Mun, S.-H. Yang, K. Ibrahim, Y. Tomioka, and C. S. Fadley, Phys. Rev. Lett. **92**, 166401 (2004); N. Mannella, W. L. Yang, K. Tanaka, X. J. Zhou, H. Zheng, J. F. Mitchell, J. Zaanen, T. P. Devereaux, N. Nagaosa, Z. Hussain, and Z.-X. Shen, Phys. Rev. B **76**, 233102 (2007).
[5] J. P. Hague, P. E. Kornilovitch, A. S. Alexandrov, and J. H. Samson, Phys. Rev. B **73**, 054303 (2006).
[6] V. N. Strocov, J. Electron Spectrosc. Relat. Phenom. **130**, 65 (2003).
[7] J. Krempaský, V. N. Strocov, L. Patthey, P. R. Willmott, R. Herger, M. Falub, P. Blaha, M. Hoesch, V. Petrov, M. C. Richter, O. Heckmann, and K. Hricovini, Phys. Rev. B **77**, 165120 (2008).
[8] J. Krempaský, V. N. Strocov, P. Blaha, L. Patthey, M. Radović, M. Falub, M. Shi, and K. Hricovini, J. Electron Spectrosc. Relat. Phenom. **181**, 63 (2010).
[9] M. Shi, M. C. Falub, P. R. Willmott, J. Krempasky, R. Herger, K. Hricovini, and L. Patthey, Phys. Rev. B **70**, 140407 (2004).
[10] A. Chikamatsu, H. Wadati, H. Kumigashira, M. Oshima, A. Fujimori, N. Hamada, T. Ohnishi, M. Lippmaa, K. Ono, M. Kawasaki, and H. Koinuma, Phys. Rev. B **73**, 195105 (2006); A. Chikamatsu, H. Wadati, H. Kumigashira, M. Oshima, A. Fujimori, M. Lippmaa, K. Ono, M. Kawasaki, and H. Koinuma, Phys. Rev. B **76**, 201103 (2007).
[11] K. Horiba, H. Ohguchi, H. Kumigashira, M. Oshima, K. Ono, N. Nakagawa, M. Lippmaa, M. Kawasaki, and H. Koinuma, Rev. Sci. Instrum. **74**, 3406 (2003); K. Horiba, A. Chikamatsu, H. Kumigashira, M. Oshima, N. Nakagawa, M. Lippmaa, K. Ono, M. Kawasaki, and H. Koinuma, Phys. Rev. B **71**, 155420 (2005).
[12] L. L. Lev, M. B. Tsetlin, M. Leandersson, A. A. Zakharov, M. N. Mikheeva, I. Lindau, and A. M. Balbashev, J. Electron Spectrosc. Relat. Phenom. **137–140**, 499 (2004).
[13] D. Pesquera, G. Herranz, A. Barla, E. Pellegrin, F. Bondino, E. Magnano, F. Sánchez, and J. Fontcuberta, Nat. Commun. **3**, 1189 (2012).
[14] A. Damascelli, Z. Hussain, and Z.-X. Shen, Rev. Mod. Phys. **75**, 473 (2003).
[15] V. N. Strocov, M. Kobayashi, X. Wang, L. L. Lev, J. Krempasky, V. V. Rogalev, T. Schmitt, C. Cancellieri, and M. L. Reinle-Schmitt, Synchrotron Radiat. News **27**, 31 (2014).
[16] V. N. Strocov, X. Wang, M. Shi, M. Kobayashi, J. Krempasky, C. Hess, T. Schmitt, and L. Patthey, J. Synchrotron Radiat. **21**, 32 (2014).
[17] J. Braun, J. Minár, S. Mankovsky, V. N. Strocov, N. B. Brookes, L. Plucinski, C. M. Schneider, C. S. Fadley, and H. Ebert, Phys. Rev. B **88**, 205409 (2013).
[18] A. A. Mukhin, V. Y. Ivanov, V. D. Travkin, S. P. Lebedev, A. Pimenov, A. Loidl, and A. M. Balbashov, J. Exp. Theor. Phys. Lett. **68**, 356 (1998).
[19] See the Supplemental Material at http://link.aps.org/supplemental/10.1103/PhysRevLett.114.237601 for additional information on the raw SX-ARPES data, its comparison with VUV-ARPES data and temperature dependence to distinguish the QP peak from the polaronic hump, linear dichroism relaxation due to the RH distortion, as well as the experimental x-ray diffraction data and structural parameters.
[20] Y. Tokura, Science **288**, 462 (2000).
[21] H. Ebert, D. Ködderitzsch, and J. Minár, Rep. Prog. Phys. **74**, 096501 (2011).
[22] P. Aebi, J. Osterwalder, P. Schwaller, L. Schlapbach, M. Shimoda, T. Mochiku, and K. Kadowaki, Phys. Rev. Lett. **72**, 2757 (1994).
[23] A. Mans, I. Santoso, Y. Huang, W. K. Siu, S. Tavaddod, V. Arpiainen, M. Lindroos, H. Berger, V. N. Strocov, M. Shi, L. Patthey, and M. S. Golden, Phys. Rev. Lett. **96**, 107007 (2006).
[24] S.-W. Cheong and H. Y. Hwang, in Colossal Magnetoresistive Oxides, edited by Y. Tokura (Gordon and Breach, London, 2000), p. 237
[25] V. E. Naish, Phys. Met. Metallogr. **85**, 589 (1998).
[26] J. Braun, Rep. Prog. Phys. **59**, 1267 (1996).
[27] A. Gray, J. Minár, S. Ueda, P. R. Stone, Y. Yamashita, J. Fujii, J. Braun, L. Plucinski, C. M. Schneider, G. Panaccione, H. Ebert, O. D. Dubon, K. Kobayashi, and C. S. Fadley, Nat. Mater. **11**, 957 (2012).
[28] V. Popescu and A. Zunger, *Phys. Rev. Lett.* 104, 236403 (2010).